Title

Functional Diversity of Cytotoxic tRNase/Immunity Protein Complexes from Burkholderia pseudomallei *

Journal

Journal of Biological Chemistry, 291(37)

ISSN

0021-9258

Authors

Johnson, Parker M

Gucinski, Grant C

Garza-Sánchez, Fernando

et al.

Publication Date

2016-09-01

DOI

10.1074/jbc.m116.736074

Peer reviewed

THE JOURNAL OF BIOLOGICAL CHEMISTRY VOL. 291, NO. 37, pp. 19387–19400, September 9, 2016
Published in the U.S.A.

Functional Diversity of Cytotoxic tRNase/Immunity Protein Complexes from *Burkholderia pseudomallei*[*]

Received for publication, May 3, 2016, and in revised form, July 18, 2016 Published, JBC Papers in Press, July 20, 2016, DOI 10.1074/jbc.M116.736074

Parker M. Johnson[‡1], Grant C. Gucinski[§], Fernando Garza-Sánchez[¶], Timothy Wong[‡], Li-Wei Hung[‖], Christopher S. Hayes[§¶2], and Celia W. Goulding[‡3]**

*From the Departments of [‡]Molecular Biology and Biochemistry and **Pharmaceutical Sciences, University of California at Irvine, Irvine, California 92697, the [§]Biomolecular Science and Engineering Program and [¶]Department of Molecular, Cellular and Developmental Biology, University of California at Santa Barbara, Santa Barbara, California 93106-9625, and the [‖]Physics Division, Los Alamos National Laboratory, Los Alamos, New Mexico 87545*

Contact-dependent growth inhibition (CDI) is a widespread mechanism of inter-bacterial competition. CDI$^+$ bacteria deploy large CdiA effector proteins, which carry variable C-terminal toxin domains (CdiA-CT). CDI$^+$ cells also produce CdiI immunity proteins that specifically neutralize cognate CdiA-CT toxins to prevent auto-inhibition. Here, we present the crystal structure of the CdiA-CT/CdiI^{E479} toxin/immunity protein complex from *Burkholderia pseudomallei* isolate E479. The CdiA-CT^{E479} tRNase domain contains a core α/β-fold that is characteristic of PD(D/E)*X*K superfamily nucleases. Unexpectedly, the closest structural homolog of CdiA-CT^{E479} is another CDI toxin domain from *B. pseudomallei* 1026b. Although unrelated in sequence, the two *B. pseudomallei* nuclease domains share similar folds and active-site architectures. By contrast, the CdiI^{E479} and CdiI^{1026b} immunity proteins share no significant sequence or structural homology. CdiA-CT^{E479} and CdiA-CT^{1026b} are both tRNases; however, each nuclease cleaves tRNA at a distinct position. We used a molecular docking approach to model each toxin bound to tRNA substrate. The resulting models fit into electron density envelopes generated by small-angle x-ray scattering analysis of catalytically inactive toxin domains bound stably to tRNA. CdiA-CT^{E479} is the third CDI toxin found to have structural homology to the PD(D/E)*X*K superfamily. We propose that CDI systems exploit the inherent sequence variability and active-site plasticity of PD(D/E)*X*K nucleases to generate toxin diversity. These findings raise the possibility that many other uncharacterized CDI toxins may belong to the PD(D/E)*X*K superfamily.

Bacterial contact-dependent growth inhibition (CDI)[4] is an important mechanism of intercellular competition in which Gram-negative bacteria intoxicate neighboring cells upon direct contact. Genes encoding CDI systems are distributed throughout α-, β-, and γ-proteobacteria and are commonly found in human pathogens such as enterohemorrhagic *Escherichia coli*, *Neisseria meningitidis, Pseudomonas aeruginosa,* and *Burkholderia pseudomallei* (1–3). CDI is a function of the CdiB/CdiA family of two-partner secretion systems. CdiB is an Omp85 β-barrel protein required for the export and display of CdiA effectors on the cell surface. Based on its homology to filamentous hemagglutinin from *Bordetella* species, CdiA proteins are predicted to form filaments that project several hundred Å from the cell surface (3–5). Upon binding to specific receptors on susceptible bacteria, CdiA delivers its C-terminal toxin domain (CdiA-CT) into the target cell to inhibit growth (6–8). CDI$^+$ bacteria are protected from toxicity by CdiI immunity proteins, which bind to the CdiA-CT toxin domain and neutralize its activity. Although the general architecture of CdiA proteins is conserved across bacteria, the effectors vary considerably in size (180–640 kDa), and CdiA-CT toxin sequences are remarkably diverse (1, 2, 9–13). Thus, CdiA effectors collectively deploy a variety of toxin domains with distinct biochemical activities (1, 3, 14, 15). Moreover, CdiI immunity proteins are also highly variable in sequence and only protect cells against cognate CdiA-CT toxins. The polymorphic nature of CDI toxin/immunity protein pairs and the specificity of their binding interactions suggest that the systems mediate inter-strain competition and self/nonself recognition.

We previously characterized CdiA-CT/CdiI pairs from environmental isolates of *Burkholderia pseudomallei*, using these systems as a model to explore toxin/immunity protein structure and evolution (16, 17). *B. pseudomallei* is a category B pathogen and the causative agent of melioidosis, a serious human disease endemic to southeast Asia and northern Australia (18, 19). *B. pseudomallei* isolates are genetically heterogeneous, and different strains are thought to compete with one another for growth niches and other resources (20, 21). CDI may contribute to inter-strain competition because every *B. pseudomallei* isolate carries at least one *cdi* gene cluster (16). *B. pseudomallei* CdiA proteins share 59–99.5% pairwise sequence identity over the N-terminal 2,770–2,829 residues

* This work was supported in part by National Institutes of Health Grants AI099687 and GM102318 (to C. W. G. and C. S. H.) and National Institutes of Health Project MINOS Grant GM105404. The authors declare that they have no conflicts of interest with the contents of this article. The content is solely the responsibility of the authors and does not necessarily represent the official views of the National Institutes of Health.

The atomic coordinates and structure factors (code 5J4A) have been deposited in the Protein Data Bank (http://wwpdb.org/).

[1] Supported in part by University of California at Irvine Bridge Funding.

[2] To whom correspondence may be addressed. Tel.: 805-893-2028; E-mail: chayes@lifesci.ucsb.edu.

[3] To whom correspondence may be addressed. Tel.: 949-824-0337; Fax: 949-824-8551; E-mail: celia.goulding@uci.edu.

[4] The abbreviations used are: CDI, contact-dependent growth inhibition; r.m.s.d., root-mean-square deviation; SAXS, small-angle x-ray scattering; SeMet, selenomethionine; SAD, single-wavelength anomalous dataset; NSD, normalized spatial discrepancy; for, forward; rev, reverse; PDB, Protein Data Bank.

but diverge abruptly after a conserved (E/Q)LYN peptide motif that demarcates the CdiA-CT region. At least 10 distinct CdiA-CT/CdiI sequence types are found in the species, but only three toxin activities have been characterized experimentally (16). The type I CdiA-CT is homologous to the nuclease domain from colicin E5 and exhibits anticodon nuclease activity against $tRNA^{His}$, $tRNA^{Tyr}$, $tRNA^{Asp}$, and $tRNA^{Asn}$ (16, 22). The type II toxin cleaves all tRNAs between conserved residues T54 and Ψ55 in the T-loop; and the type V toxin preferentially cleaves near the 3′-end of $tRNA^{Ala}$ (16, 17). Type VII and VIII CdiA-CT sequences are closely related in sequence and are predicted RNA deaminases (14). There are no predicted activities for the other *B. pseudomallei* CDI toxins, although the type X toxin contains a conserved RES (Arg-Glu-Ser) domain of unknown function (Pfam: PF08808).

Here, we present the crystal structure of the type II toxin/immunity protein complex from *B. pseudomallei* isolate E479 (16, 20). The C-terminal tRNase domain of CdiA-CT^{E479} is built upon an α/β-fold characteristic of PD(D/E)*X*K nucleases. The PD(D/E)*X*K superfamily includes most restriction endonucleases and other enzymes involved in DNA recombination and repair (23). A DALI server (24) search reveals that the type V toxin domain from *B. pseudomallei* 1026b is the closest structural homolog of CdiA-CT^{E479}. Although CdiA-CT^{E479} and CdiA-CT^{1026b} nuclease domains do not share significant sequence identity, they have very similar active-site architectures with catalytic residues contributed by α1, β2, β3, and α2 elements of the PD(D/E)*X*K core. By contrast, $CdiI^{E479}$ and $CdiI^{1026b}$ are unrelated in sequence and structure, but each immunity protein inactivates cognate toxin by binding within the nuclease active-site cleft to prevent access to tRNA. To gain insight into substrate specificity, we used molecular docking approaches to model each toxin domain bound to tRNA. The resulting models fit reasonably well into low resolution electron-density envelopes generated by small-angle x-ray scattering analysis of toxin/tRNA complexes. Although most PD(D/E)*X*K nucleases are DNA-specific phosphodiesterases, our findings indicate that these enzymes are commonly used as toxic RNases in bacterial competition. Because PD(D/E)*X*K nucleases can be difficult to identify through sequence analyses (23, 25), it is possible that many other uncharacterized CDI toxins also belong to the superfamily.

Results

Structure of the CdiA-CT/$CdiI^{E479}$ Toxin/Immunity Protein Complex—We previously reported that overexpression of the CdiA-CT/$CdiI^{E479}$/His_6 complex in *E. coli* cells leads to tRNA degradation and concomitant growth arrest (16). These observations suggest that the expression construct produces insufficient immunity protein to neutralize tRNase activity. Because CdiA-CT^{E479} activity precludes protein overproduction, we inactivated the toxin with the D285A mutation to allow high level expression of the toxin/immunity protein complex (16). We purified and crystallized the SeMet-labeled complex and used SAD phasing to produce an initial partial model. The model was subsequently improved using molecular replacement with a native dataset, resulting in a final resolution of 2.0 Å (Table 1). The final model includes CdiA-CT^{E479} residues Arg-201–Lys-316 (numbered from Glu-1 of the ELYN peptide motif), $CdiI^{E479}$ residues Ala-2–Gly-105, and 155 water molecules. The final R_{work}/R_{free} (%) was 19.3/23.7 with 98.8% of dihedral angles in favorable regions and the remaining 1.2% within allowed regions as estimated by Ramachandran plot.

Like other CdiA-CT constructs (17, 26, 27), the N-terminal region of CdiA-CT^{E479} (residues Glu-1–Phe-200) is not resolved in the final model. This unresolved region corresponds to the "translocation" domain, which is postulated to mediate CdiA-CT transport across the cytoplasmic membrane of target bacteria (28). The resolved C-terminal domain corresponds to the tRNase domain responsible for growth inhibition activity (16). The CdiA-CT^{E479} nuclease domain consists of a five-stranded mixed β-sheet decorated by four α-helices (Fig. 1*A*). The sheet forms a half β-barrel-like structure with helix α1 running through its central cavity (Fig. 1*A*). The C-terminal half of helix α2 (α2b) is bent 90° with respect to the N-terminal portion (α2a). The $CdiI^{E479}$ immunity protein consists of a slightly curved three-stranded antiparallel β-sheet decorated with four α-helices (Fig. 1*A*). The CdiA-CT/$CdiI^{E479}$ interface is largely electrostatic with 19 direct salt bridges and hydrogen bonds mediating the interaction (Fig. 1*B* and Table 2). Helix α2b of the nuclease domain sits in the curve of the $CdiI^{E479}$ β-sheet. Additionally, helices α1′, α4′, and the β-sheet of $CdiI^{E479}$ interact with the end of the nuclease β-sheet and the extended loop connecting α2′ and β3′ (Fig. 1*B*). This protein-protein interface buries 1015 $Å^2$ of surface area, corresponding to 14% of the nuclease domain and 18% of the immunity protein total surface area. In accord with this extensive interaction surface, biolayer interferometry showed that CdiA-CT^{E479} and $CdiI^{E479}$ form a relatively high affinity complex with an apparent equilibrium dissociation constant of 72 ± 23 nM (Fig. 2).

CdiA-CT^{E479} Toxin Domain Is a Member of the PD(D/E)XK Superfamily—We used the DALI server (24) to identify proteins with structural similarity to the CdiA-CT^{E479} nuclease domain. This search revealed that two other CdiA-CT nuclease domains from *B. pseudomallei* 1026b and *Yersinia pseudotuberculosis* YPIII exhibit the greatest similarity with CdiA-CT^{E479} (Table 3). The CdiA-CT^{1026b} and CdiA-CT^{E479} nuclease domains superimpose with a root-mean-square deviation (r.m.s.d.) of 3.7 Å over 89 of 132 α-carbons, corresponding to a DALI *Z*-score of 7.0. The CdiA-CT^{YPIII} nuclease domain exhibits comparable structural similarity, although its β4-β5 hairpin element is absent from the CdiA-CT^{E479} nuclease domain (27). Other proteins identified during this search include two closely related XisH endonucleases from cyanobacteria, another CdiA-CT nuclease domain from *Escherichia coli* EC869, and the AspBHI restriction endonuclease from *Azoarcus* sp. BH72 (Table 3). All of these domains share the core structure of the PD(D/E)*X*K nuclease superfamily, which includes most type II restriction endonucleases and various enzymes involved in DNA recombination and repair. The PD(D/E)*X*K core domain is a mixed β-sheet flanked by two α-helices with αββββαβ topology. CdiA-CT^{E479} and CdiA-CT^{1026b} share this core fold, but the CdiA-CT^{E479} nuclease domain contains an insertion that forms helix α2a (Fig. 3, *A* and *B*). We also note that helix α1 from CdiA-CT^{E479} is significantly

TABLE 1
X-ray diffraction data and atomic refinement for the CdiA-CT·CdiI^{E479} complex
NA means not applicable.

	Se-SAD dataset	Native dataset
Space group	*I*4	$P22_12_1$
Unit cell dimensions (Å)	117.2 × 117.2 × 111.6	54.5 × 73.3 × 110.0
pH of crystallization condition	6.5	7.0
Protein concentration (mg/ml)	20	20
Dataset		
Wavelength, Å	0.97591	0.97591
Resolution range	50–3.3	50–2.0
Unique reflections (total)	22,290 (329,892)	30,121 (322,487)
Completeness, %[a]	100 (100)	99.24 (99.28)
Redundancy[a]	14.8 (14.9)	10.7 (10.9)
R_{merge}[a,b]	0.159 (0.48)	0.071 (0.494)
R_{meas}[a,c]	0.157 (0.467)	0.075 (0.519)
$R_{p.i.m.}$[a,d]	0.041 (0.121)	0.023 (0.156)
$CC_{1/2}$[a]	0.999 (0.993)	0.998 (0.966)
I/σ[a]	18.03 (6.95)	29.99 (5.79)
Figure of merit	0.408	NA
No. of selenium sites	18	NA
NCS copies	3	2
Model refinement		
Resolution range, Å		43.7–2.0
No. of reflections (working/free)		30,094
No. of protein atoms		3,382
No. of water molecules		155
Residues in model		CdiA-CT 201–316; CdiI 2–105
R_{work}/R_{free} %[e]		19.3/23.7
Room mean square deviations		
Bond lengths, Å		0.008
Bond angles		1.09
Ramachandran plot		
Most favorable region, %		98.8
Additional allowed region, %		1.2
Disallowed region		0
PDB code		5J4A

[a] Statistics for the highest resolution shell are given in parentheses.
[b] $R_{merge} = \Sigma_{hkl}\Sigma_i|I_i(hkl) - (I(hkl))|/\Sigma_{hkl}\Sigma_i I_i(hkl)$.
[c] $R_{meas} = \Sigma_{hkl}\{N(hkl)/(N(hkl) - 1)\}^{1/2}\Sigma_i|I_i(hkl) - (I(hkl))|/\Sigma_{hkl}\Sigma_i I_i(hkl)$.
[d] $R_{p.i.m}$ (precision-indicating R_{merge}) $= \Sigma_{hkl}\{1/(N(hkl) - 1)\}^{1/2}\Sigma_i|I_i(hkl) - (I(hkl))|/\Sigma_{hkl}\Sigma_i I_i(hkl)$.
[e] $R_{work} = \Sigma|F_{obs} - F_{calc}|/\Sigma F_{obs}$. R_{free} was computed identically except where all reflections belong to a test set of 5% randomly selected data.

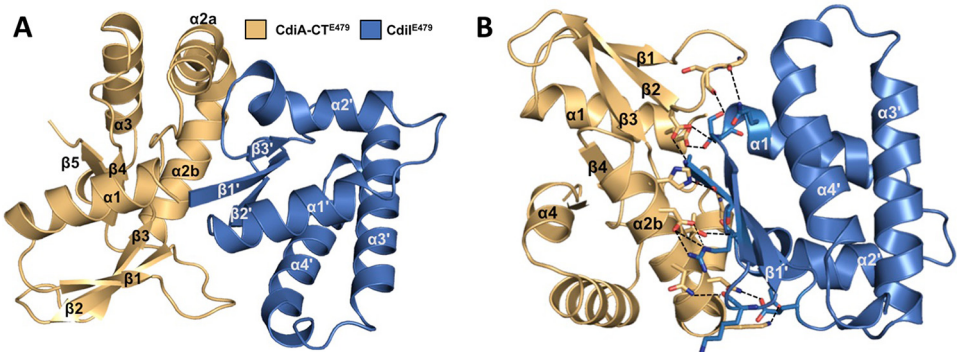

FIGURE 1. **Structure of the CdiA-CT/CdiI^{E479} toxin/immunity protein complex.** *A*, CdiA-CT/CdiI^{E479} complex is shown as a schematic with secondary structure elements of CdiI indicated with prime symbols. *B*, CdiA-CT/CdiI^{E479} complex formation is mediated by electrostatic interactions. Interacting residues are in *stick* representation with nitrogen and oxygen atoms colored in *blue* and *red* (respectively), and bonds are shown as *black dashed lines*. The view is rotated 180° about the *x* axis relative to *A*.

shorter than the corresponding helix in the CdiA-CT^{1026b} structure (Fig. 3, *A* and *B*).

Identification of the CdiA-CT^{E479} Active Site—We previously suggested that Asp-280 and Asp-285 of CdiA-CT^{E479} may function in catalysis, because mutation of these residues abrogated toxicity (16). However, structural alignment with the nuclease domain from CdiA-CT^{1026b} indicates that residues Glu-204, Asp-229, Asp-243, and His-275 of CdiA-CT^{E479} are more likely to catalyze tRNA cleavage (Fig. 3*A*). These residues overlay well with active-site residues Glu-187, Asp-214, Asp-223, and Lys-242 of CdiA-CT^{1026b} (Fig. 3*C*). To test this prediction, we mutated CdiA-CT^{E479} residues His-275, Asp-243, Asp-229, and Glu-204 to Ala individually and examined the growth inhibition activity of each toxin variant. Induction of wild-type CdiA-CT^{E479} expression in *E. coli* cells resulted in immediate growth inhibition (Fig. 4*A*). By contrast, induction of domains that carry the H275A, D243A, D229A, or E204A mutations had no effect on cell growth (Fig. 4*A*), consistent with the loss of toxic nuclease activity. We also purified each toxin domain and tested its tRNase activity *in vitro*. Wild-type CdiA-CT^{E479} toxin

cleaved a large proportion of tRNA molecules as assessed by denaturing PAGE analysis, and this activity was blocked when purified CdiI^{E479} immunity protein was included in the reaction (Fig. 4*B*). This tRNase activity was confirmed by Northern blot analysis, which showed cleavage of tRNA^{Gly} molecules in the reactions (Fig. 4*B*). By contrast, none of the other CdiA-CT^{E479} mutant variants exhibited detectable RNase activity (Fig. 4*B*).

TABLE 2

Direct intermolecular hydrogen bonds and salt bridges in the CdiA-CT·CdiI^{E479} complex

CdiA-CT^{E479}	CdiI^{E479}	Distance
		Å
Hydrogen bonds		
Glu-204(OE2)	Thr-17 (OG1)	2.39
Gly-225(O)	Gln-19 (NE2)	3.79
Ser-226(O)	Ser-16 (NE2)	3.37
Asp-229(OD1)	Thr-17(N)	2.79
Gln-253(NE2)	Gly-50(O)	2.98
Asn-267(ND2)	Glu-57 (OE2)	2.66
Asn-270(ND2)	Lys-9(O)	3.70
Thr-271(OG1)	Ser-4(OG)	2.39
His-275(NE2)	Gly-3(O)	2.62
Salt bridges		
Asp-229(OD2)	Ala-2(N)	3.83
Lys-263(NZ)	Glu-48 (OE1)	3.64
Lys-263(NZ)	Glu-48 (OE2)	2.47
Asp-274(OD1)	Arg-12(NE)	3.78
Asp-274(OD2)	Arg-12(NE)	2.82
Asp-274(OD1)	Arg-12 (NH_2)	2.97
Asp-274(OD2)	Arg-12 (NH_2)	3.47

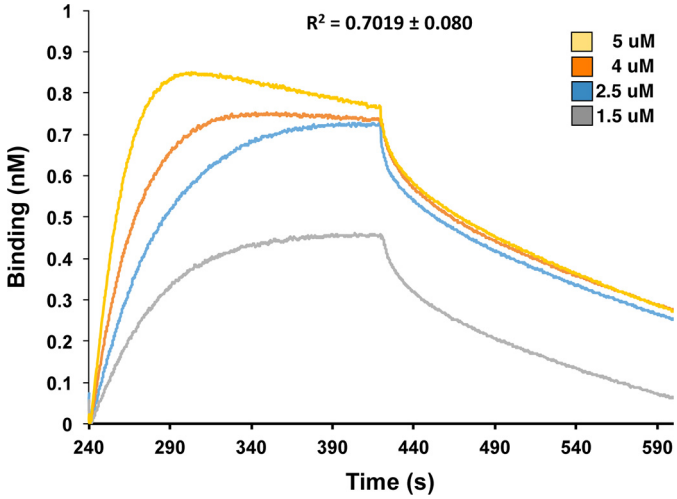

FIGURE 2. **Biolayer interferometry of the CdiA-CT/CdiI^{E479} binding interaction.** Immobilized CdiI^{E479}-His_6 was exposed to varying concentrations (1.5–5 μM) of CdiA-CT^{E479}, and the binding interaction and dissociation monitored a wavelength shift (nm). Representative association and dissociation curves are presented with the overall correlation coefficient (R^2) shown for the fit.

To determine whether the mutations adversely affect toxin structure, we tested whether the refolded CdiA-CT^{E479} proteins still interact with cognate immunity protein using affinity co-purification. Each mutant toxin co-eluted with CdiI^{E479}-His_6 during Ni^{2+}-affinity chromatography (Fig. 4*C*), indicating that the nuclease domains retain their native fold. Taken together with the crystal structure, these findings suggest that CdiA-CT^{E479} residues His-275, Asp-243, Asp-229, and Glu-204 participate in catalysis. Because CdiI^{E479} binds directly over this cluster of residues, the immunity protein presumably neutralizes toxin activity by blocking access to tRNA substrates. We previously showed that CdiA-CT^{E479} cleaves between residues T54 and Ψ55 in the T-loop of tRNA molecules (16). To test whether post-transcriptional modifications at positions 54 and 55 are required for CdiA-CT^{E479} activity, we examined toxin activity on unmodified *E. coli* tRNA^{Asp} and tRNA^{Gln} substrates prepared by *in vitro* transcription. Each substrate was cleaved efficiently by purified nuclease and the activity completely neutralized by CdiI^{E479} immunity protein (Fig. 4*D*). Thus, the universal T-loop modifications are not required for CdiA-CT^{E479}-mediated tRNase activity.

Structural Comparison of CdiI^{E479} and CdiI^{1026b} Immunity Proteins—Although the CdiA-CT^{E479} and CdiA-CT^{1026b} nuclease domains share a common fold and active site, the corresponding immunity proteins appear to be unrelated. Using iterative PSI-BLAST, we were unable to establish a link between CdiI^{E479} and CdiI^{1026b} sequences. Moreover, structural superimposition of the two immunity proteins reveals a poor fit between the central β-sheets and misalignments of most α-helical elements (Fig. 5, *A* and *B*). CdiI^{E479} and CdiI^{1026b} align with an r.m.s.d. of 3.42 Å over only 42 of 103 α-carbons (*Z*-score of 1.8) indicating low structural similarity. We next used the DALI server to search for proteins with structural similarity to CdiI^{E479}. The only hit with a *Z*-score of >5 was the N-terminal domain of protein NS3 from rice hoja blanca tenuivirus (Table 3). NS3 suppresses RNA interference pathways in host cells by binding to both siRNA and miRNAs (29, 30). Although these proteins superimpose with r.m.s.d. of 2.7 Å over 75 of 90 α-carbons, the NS3 domain is entirely α-helical and lacks the central β-sheet found in CdiI^{E479}.

CdiA-CT/CdiI Complexes Have Unique Electrostatic Interfaces—Both toxin/immunity complexes interact primarily via electrostatic interactions and shape complementation; and intriguingly, both immunity proteins use the N-terminal α-amino group to form a salt bridge with a catalytic Asp residue in the toxin active site (Table 2) (17). However, the size, charge distribution, shape, and position of these patches differ between the two immunity proteins (Fig. 6). The electrostatic

TABLE 3

DALI server search results

Search input	Structural homolog	Organism	PDB code	*Z*-score	r.m.s.d.[a]
					Å
CdiA-CT^{E479}	CdiA-CT$_{II}^{1026b}$	*B. pseudomallei* 1026b	4G6V	7.0	3.7 (89/132)[b]
	CdiA-CT^{YPIII}	*Y. pseudotuberculosis* YPIII	4ZQU	7.0	3.0 (95/124)
	XisH	*Nostoc punctiforme* PCC 73102	2INB	6.4	2.7 (87/128)
	AVA_3312	*Anabaena variabilis*	2OKF	6.4	2.9 (90/129)
	CdiA-CT$_{o11}^{EC869}$	*E. coli* EC869	4G6U	5.8	3.3 (96/213)
	AspBHI	*Azoarcus* sp. BH72	4OC8	5.2	3.2 (91/387)
CdiI^{E479}	NS3	Rice hoja blanca virus (RHBV)	3AJF	5.8	2.7 (75/90)

[a] r.m.s.d. is root-mean-square deviation.
[b] Data were aligned over number of α-carbons out of number of residues.

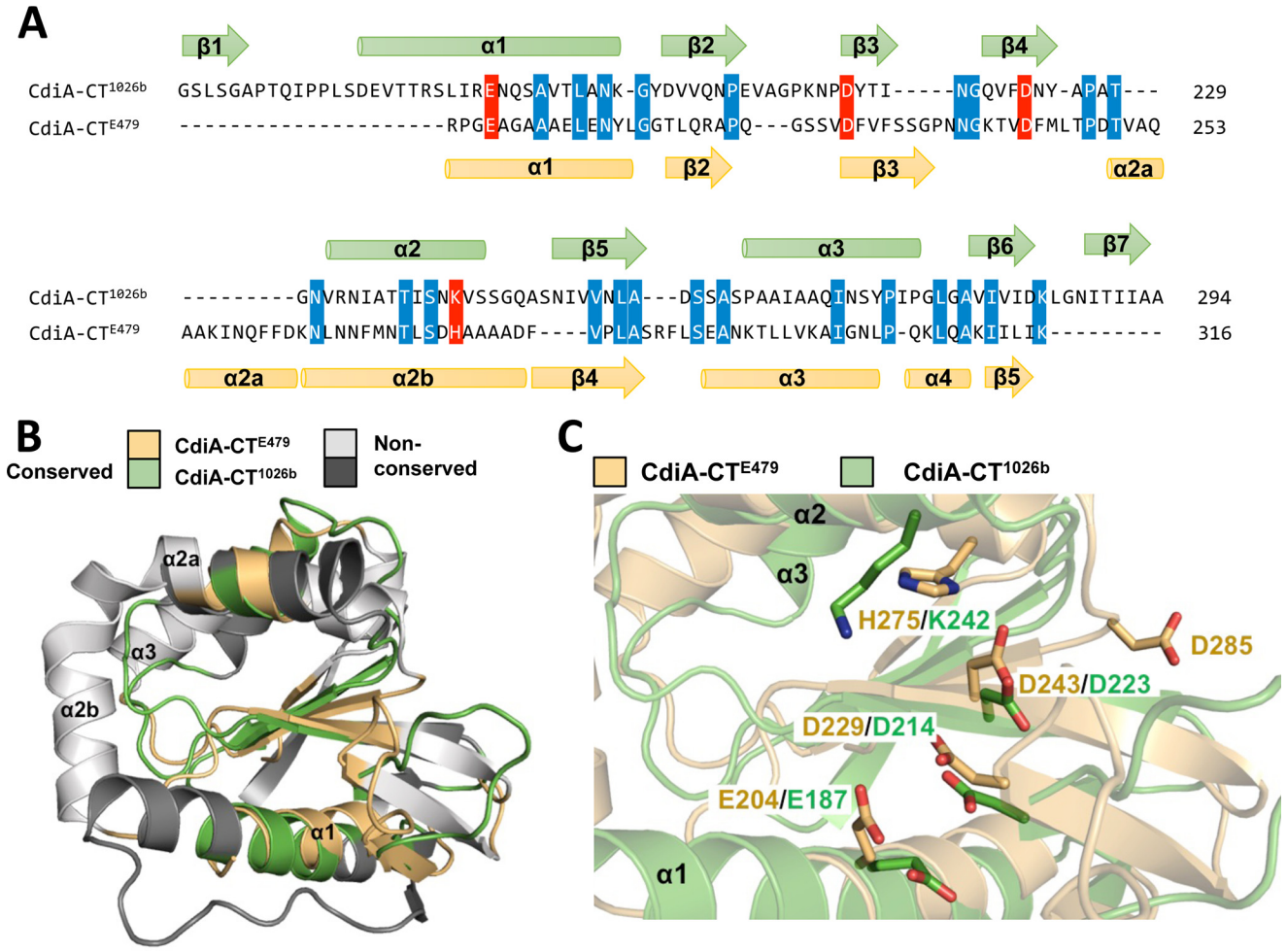

FIGURE 3. **Sequence and structure alignment of CdiA-CT^{E479} and CdiA-CT^{1026b} nuclease domains.** *A,* sequence alignment of CdiA-CT^{E479} and CdiA-CT^{1026b} toxins with proposed active-site residues highlighted in *red* and conserved residues in *blue*. Secondary structure elements are colored *gold* and *green* for CdiA-CT^{E479} and CdiA-CT^{1026b}, respectively. *B,* superimposition of CdiA-CT^{E479} and CdiA-CT^{1026b} nuclease domains. Secondary structure elements that superimpose are color-coded in *gold* (CdiA-CT^{E479}) and *green* (CdiA-CT^{1026b}), and those that do not align rendered in *white* (CdiA-CT^{E479}) and *gray* (CdiA-CT^{1026b}). *C,* active site of CdiA-CT^{E479} and CdiA-CT^{1026b} nuclease domain. Predicted active-site residues are shown in *stick* representation (nitrogen and oxygen atoms are colored *blue* and *red*, respectively).

surface map shows that CdiI^{E479} has a positively charged protrusion (formed from α1′, α2′, and the β-sheet) that is complementary to the negatively charged active-site groove within the CdiA-CT^{E479} nuclease domain (Fig. 6*A*). In addition, a small negatively charged patch on CdiI^{E479} interacts with a positive patch on the cognate toxin. Much like CdiI^{E479}, the CdiI^{1026b} immunity protein inserts a positively charged protrusion (formed from β3′, α3′, and the connecting loop region) into the negatively charged active-site cleft of its cognate toxin. CdiI^{1026b} also contains a negatively charged patch, which complements a positive patch adjacent to the Lys-242 active-site residue within CdiA-CT^{1026b}. Collectively, these electrostatic and shape complementation interactions ensure that each nuclease domain is only neutralized by its cognate immunity protein.

Nuclease Active-site Architecture and tRNA Specificity—CdiA-CT^{E479} and CdiA-CT^{1026b} cleave tRNA at distinct positions, and presumably, this specificity is dictated by the shape of the active-site pocket. The CdiA-CT^{E479} nuclease domain has a slightly larger open pocket with a diameter of 12.6 Å measured from Gln-253 to His-275 (Fig. 6*A*). By contrast, the active-site cleft of CdiA-CT^{1026b} is narrower with a diameter of 10.4 Å from Glu-187 to Lys-242 (Fig. 6*B*). To explore how the nuclease domains interact with substrate, we used Hex 8.0 to dock each toxin onto the structure of *E. coli* tRNA^{Cys}. We used experimentally determined cleavage sites for each nuclease to guide the docking searches. The models obtained from the simulations show that each nuclease active-site is positioned near the scissile bond in the tRNA substrate (Fig. 7, *A* and *C*). The calculated interaction energy for the tRNA/CdiA-CT^{E479} complex was −802 kcal/mol, and that of the tRNA/CdiA-CT^{1026b} complex was −1,267 kcal/mol. These energies are comparable with those calculated for Hex-assisted docking of each toxin domain with its cognate immunity protein as follows: −953 kcal/mol for CdiA-CT/CdiI^{E479} complex and −1,199 kcal/mol for the CdiA-CT/CdiI^{1026b} complex. A negative control simulation using CdiI^{E479} and CysK, which do not interact with one another, yielded a considerably higher energy of −368 kcal/mol. Simulations using non-cognate toxin/immunity protein pairs produced models with lower than anticipated energies (−742 kcal/mol for CdiA-CT^{E479}/CdiI^{1026b} and −626 kcal/mol for CdiA-CT^{1026b}/CdiI^{E479}), but in each instance the solutions did not position the immunity proteins over the nuclease active sites.

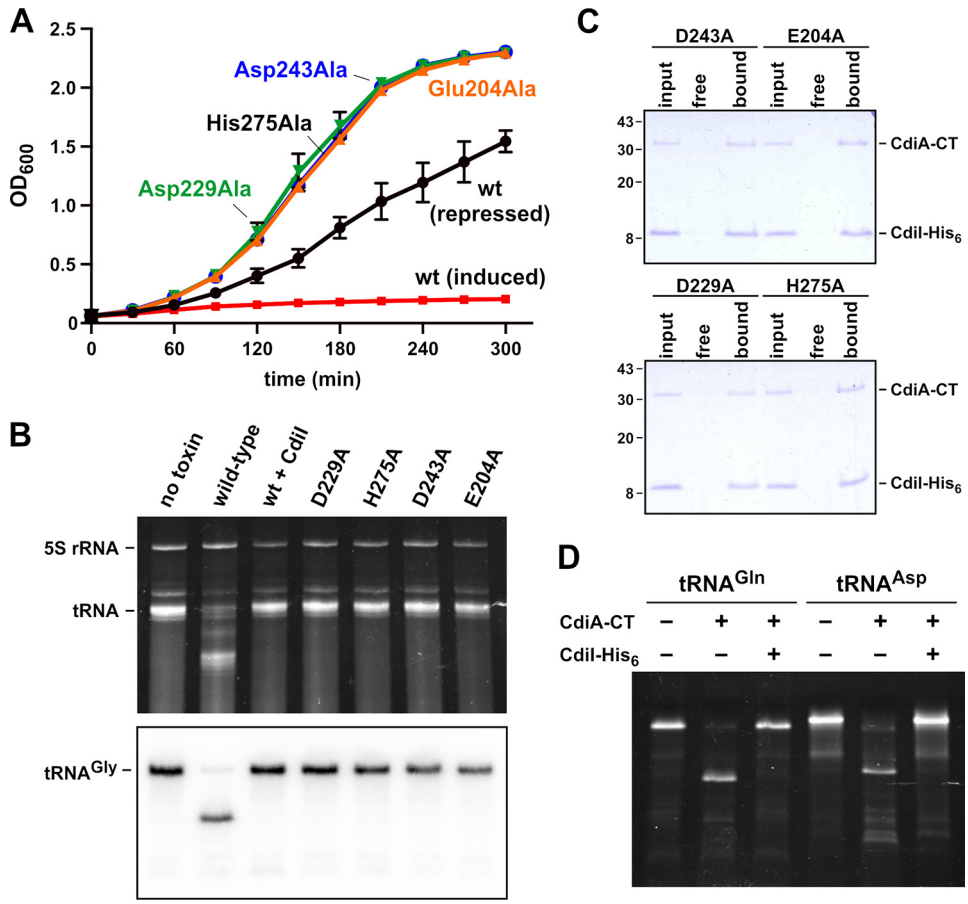

FIGURE 4. **CdiA-CT^{E479} growth inhibition and tRNase activities.** *A*, growth inhibition activity of CdiA-CT^{E479} variants. The indicated toxins were expressed in *E. coli* cells from a rhamnose-inducible promoter as described under "Experimental Procedures." Expression was induced at 0 min, and cell growth was monitored by measuring the optical density at 600 nm (OD_{600}). The *curve labeled repressed* corresponds to un-induced cells carrying the wild-type CdiA-CT^{E479} construct. The average ± S.E. from three independent biological replicates is presented. *B, in vitro* nuclease assays. The indicated CdiA-CT^{E479} variants were purified and incubated with total *E. coli* RNA. Reactions were run on denaturing 6% polyacrylamide gels and stained with ethidium bromide. *C*, mutant CdiA-CT^{E479} domains bind to CdiI^{E479} immunity protein. Isolated toxin domains were mixed with purified CdiI^{E479}-His$_6$ and then subjected to Ni^{2+}-affinity chromatography. *Lanes labeled input* show the protein mixtures loaded onto the column; *free lanes* show proteins that failed to bind the column, and *bound* indicates proteins eluted from the column with imidazole. Prior work has shown that CdiA-CT^{E479} does not bind to Ni^{2+}-NTA-agarose resin (16). *D*, CdiA-CT^{E479} cleaves unmodified tRNAs produced by *in vitro* transcription. *E. coli* tRNA^{Gln} and tRNA^{Asp} transcripts were incubated with purified CdiA-CT^{E479} and CdiI^{E479}, and reactions were analyzed on denaturing 6% polyacrylamide gels stained with ethidium bromide. Experiments in *B–D* were repeated twice with essentially identical results. Representative data are shown for each experiment.

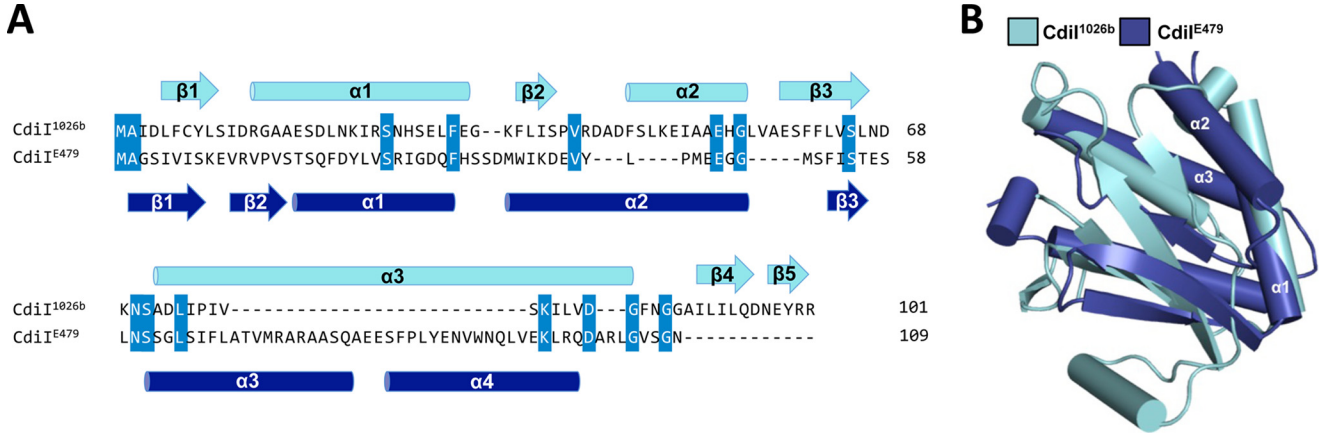

FIGURE 5. **Sequence and structure comparison of CdiI^{E479} and CdiI^{1026b} immunity proteins.** *A*, structure-based sequence alignment of CdiI^{E479} (*blue*) and CdiI^{1026b} (*cyan*) with secondary structure elements indicated *above* and *below* the sequence alignment. Conserved residues are highlighted in *blue*. *B*, superimposition of CdiI^{E479} and CdiI^{1026b} structures. Secondary elements that partially or fully superimpose are labeled.

Small-angle X-ray Scattering (SAXS) Analysis of Toxin/tRNA Complexes—To test the computational docking models, we sought to produce stable tRNA/toxin complexes for structural analysis using SAXS. We overproduced catalytically inactive toxins that carry N-terminal His$_6$ tags and purified the proteins by Ni^{2+}-affinity chromatography. Remarkably,

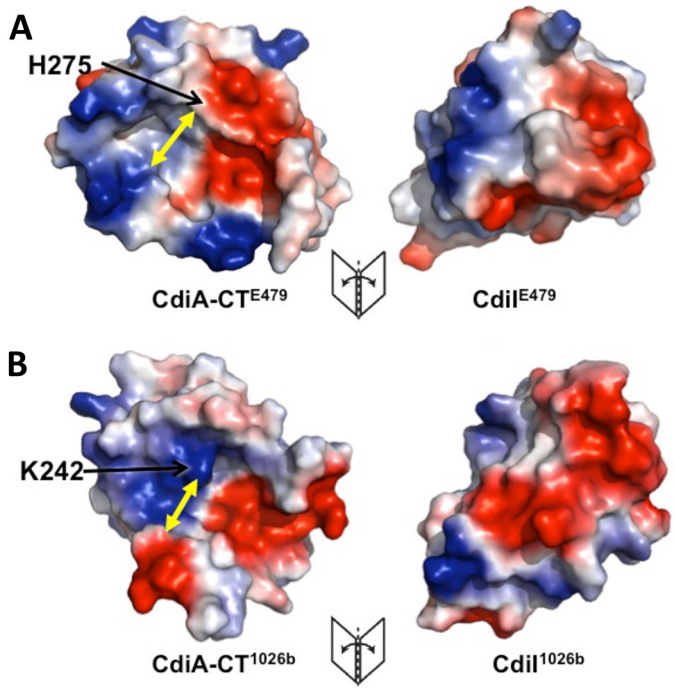

FIGURE 6. **CdiA-CT/CdiI^{E479} and CdiA-CT/CdiI^{1026b} complexes interact through distinct electrostatic surfaces.** *A,* electrostatic surface map of the CdiA-CT/CdiI^{E479} complex interface. Negative, positive, and neutral surfaces regions are shown in *red, blue,* and *white*, respectively. *B,* electrostatic surface map of the CdiA-CT/CdiI^{1026b} complex interface. *Yellow arrows* indicate the minimal width of each active-site pocket.

large quantities of endogenous tRNA co-purified with each inactive toxin (Fig. 8*A*), indicating that the tRNA/toxin complexes are indeed stable. The tRNA/CdiA-CT^{1026b} complex migrated at ~45 kDa on size-exclusion chromatography, indicative of a 1:1 complex with tRNA in solution (Fig. 8*B*). By contrast, size-exclusion chromatography showed that the tRNA/CdiA-CT^{E479} complex is ~150 kDa (Fig. 8*C*), suggestive of a higher order complex containing four nuclease domains bound to four tRNA molecules. We used SAXS to generate low resolution electron density envelopes of each nucleoprotein complex. DAMAVER (31) was used to calculate normalized spatial discrepancies (NSD) of 0.979 ± 0.038 for tRNA/CdiA-CT^{1026b} and 0.959 ± 0.081 for the tRNA/CdiA-CT^{E479} complex, with no restorations rejected. These average NSD values imply reasonable stability of the solutions. The Hex-generated models for each tRNA/toxin complex were then fitted into the respective electron density envelopes using Chimera (Fig. 7, *B* and *D*) (32). Supcomb (33) was used to calculate the NSD values between the averaged and filtered shape from SAXS and the structural models of 0.9371 for tRNA/CdiA-CT^{1026b} and 0.9013 for the tRNA/CdiA-CT^{E479} complex. These NSD values suggest that the average SAXS envelopes and the structural models agree quite well with each other. The four CdiA-CT^{E479} nuclease domains form a donut-like structure. Each nuclease domain fits helix $\alpha3$ into the curvature of the β-sheet (strands $\beta1$–$\beta3$) on the adjacent domain. Interdomain contacts also occur between helix $\alpha4$ and $\beta5$ and the loop connecting strands $\beta2$ and $\beta3$. Within the tetramer, the four $\alpha1$ helices are directed toward the center, and the nuclease active sites project outward. The buried surface area of each monomer is consistent with a stable oligomeric state (34). The complex is further stabilized by interactions between tRNA molecules, which pack together with their aminoacyl acceptor stems pointing into the center of the complex. Similar tight packing interactions have been observed in the crystal structure of tRNA^{Asp} (35).

Discussion

The results presented here demonstrate that the CdiA-CT^{E479} nuclease domain is a member of the PD(D/E)*X*K nuclease superfamily. Together with the previously characterized CdiA-CT^{1026b} and CdiA-CT$_{o11}{}^{EC869}$ nuclease domains (17, 27), there are at least three CDI toxin classes that share the PD(D/E)*X*K core fold. The amino acid sequences of these toxins are distinct (15–18% pairwise sequence identity) and show no apparent relationship to one another through iterative PSI-BLAST analyses. However, structural superimposition of the CdiA-CT^{E479}, CdiA-CT^{1026b}, and CdiA-CT$_{o11}{}^{EC869}$ toxins reveals significant similarities. The PD(D/E)*X*K fold consists of a central four-stranded mixed β-sheet flanked by two α-helices with a characteristic $\alpha_1\beta_1\beta_2\beta_3\alpha_2\beta_4$ topology. The core structure serves as a scaffold to arrange catalytic residues. The canonical PD(D/E)*X*K active site found in type II restriction endonucleases is built from a conserved Asp residue at the N terminus of $\beta2$ and the (D/E)*X*K sub-motif within $\beta3$ of the core (23, 36). However, there are several variations in the active-site configuration, with catalytic residues migrating to other secondary structure elements during evolution (23, 37, 38). For the CdiA-CT^{E479} nuclease domain, Asp-229 and Asp-243 occupy canonical positions within $\beta2$ and $\beta3$, but Glu-204 and His-275 are contributed by $\alpha1$ and $\alpha2$, respectively. This arrangement is very similar to the active site of CdiA-CT^{1026b} and the type IIS restriction endonuclease BspD6I (17, 39). The DNase domains of CdiA-CT$_{o11}{}^{EC869}$ and CdiA-CT^{YPIII} have yet another configuration that was first described for EcoO109I (17, 27, 40, 41). In these latter enzymes, Glu of the (D/E)*X*K sub-motif has migrated from $\beta3$ to helix $\alpha1$ to produce an alternative E-PD*XX*K motif. For the CdiA-CT$_{o11}{}^{EC869}$ class of toxins, the active sites use an E(F/Y)DS*X*K sequence motif (17, 27). Interestingly, these latter DNases contain an additional β-hairpin inserted between $\alpha2$ and $\beta4$ of the PD(D/E)*X*K core. This β-hairpin constitutes much of the binding interface with the cognate immunity protein, and its sequence varies between family members (27). Analogous insertions into the PD(D/E)*X*K core have been detected in other superfamily members (23), again underscoring the flexibility of the core fold.

Most PD(D/E)*X*K enzymes are phosphodiesterases involved in DNA restriction, transposon excision, recombination, and repair. By contrast, there are relatively few family members with RNase activity. EndA/Sen15 tRNA splicing endonucleases were the first PD(D/E)*X*K enzymes to be implicated in RNA metabolism (23, 42). More recently, Rai1 has been reported to act as a phosphodiesterase to remove 5′-cap structures from eukaryotic mRNAs (43). Our findings show that the PD(D/E)*X*K fold has been adopted to produce RNases with novel specificities. The CdiA-CT^{E479} nuclease domain cleaves tRNA

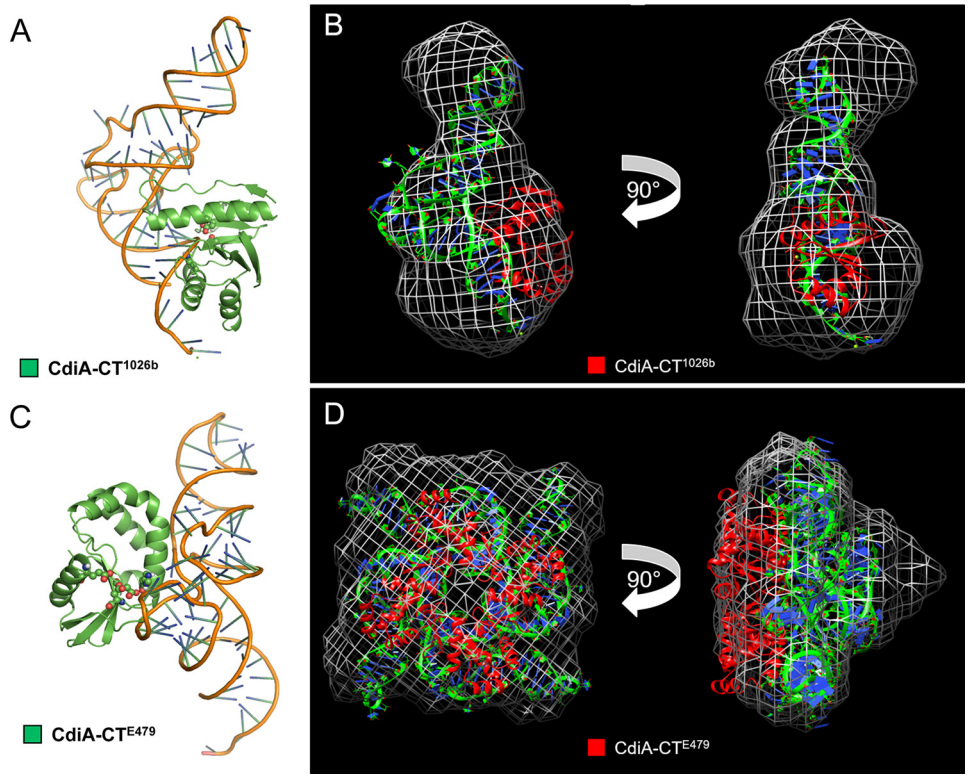

FIGURE 7. **Computational modeling and SAXS analysis of tRNA/CdiA-CT complexes.** *A,* CdiA-CT^{1026b} (*green schematic*) binding with its active-site residues adjacent to the backbone of the tRNA^{Cys} (PDB code 1B23) amino acceptor stem loop with active-site residues shown as *spheres* (oxygen and nitrogen atoms colored *red* and *blue*, respectively). *B,* SAXS electron density envelope (*white mesh*) fitted with the docking solution showing the monomeric CdiA-CT^{1026b} toxin (*red schematic*) bound to tRNA^{Cys} (*green* and *blue*). *C,* CdiA-CT^{E479} (*green schematic*) binding with its active-site residues adjacent to the backbone of the tRNA^{Cys} T-loop with active-site residues shown as *spheres* (oxygen and nitrogen atoms colored *red* and *blue*, respectively). *D,* SAXS electron density envelope (*white mesh*) fitted with the docking solution showing the tetrameric CdiA-CT^{E479} toxin bound to four molecules of tRNA^{Cys} (*green* and *blue*).

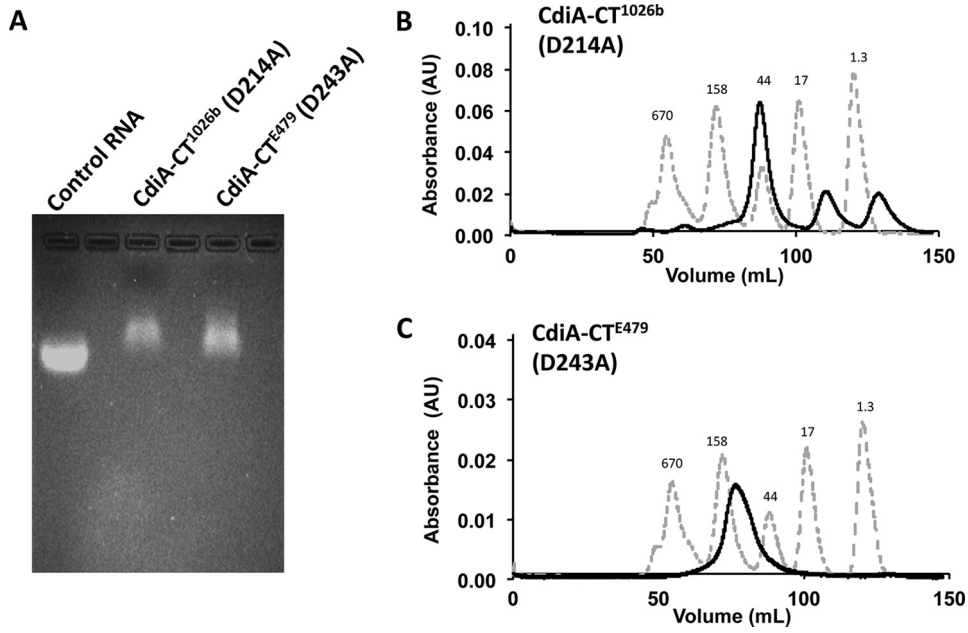

FIGURE 8. **Inactive CdiA-CT^{E479} and CdiA-CT^{1026b} toxin domains bind to endogenous tRNA.** *A,* agarose gel analysis of catalytically inactive CdiA-CT^{E479} and CdiA-CT^{1026b} toxins purified under non-denaturing conditions. Control RNA is from yeast (Sigma). *B,* size-exclusion chromatography of the purified tRNA/CdiA-CT(D214A)^{1026b} complex. *C,* size-exclusion chromatography of the purified tRNA/CdiA-CT(D243A)^{E479} complex. Chromatography migration standards are as follows: bovine thyroglobulin (670 kDa), bovine γ-globulin (158 kDa), chicken ovalbumin (44 kDa), horse myoglobin (17 kDa), and vitamin B_{12} (1.3 kDa). Each experiment was carried out in triplicate with similar results. Representative data are shown for each experiment.

between residues T54 and Ψ55 of the conserved TΨC-loop (16). Positions 54 and 55 are modified to thymidine and pseudouracil in eubacterial tRNAs, but these universal post-transcriptional modifications are not required for CdiA-CT^{E479} activity *in vitro*. CdiA-CT^{1026b} is a novel RNase that cleaves near the 3′-end of tRNA (16, 17). The computational docking

TABLE 4
Bacterial strains and plasmids

Strains or plasmids	Description[a]	Ref. or source
Strain		
BL21 (DE3)	F′ *ompT gal dcm lon hsdS$_B$* (r_B^- m_B^-)	Novagen
X90	F′ *lacI^q lac′ pro′/ara* Δ(*lac-pro*) *nal1 argE*(amb) *rif′ thi-1*, Rif^R	61
CH2016	X90 (DE3) Δ*rna* Δ*slyD*::*kan*, Rif^R Kan^R	51
Plasmids		
pET21b	Isopropyl 1-thio-β-D-galactopyranoside-inducible T7 RNA polymerase expression vector, Amp^R	Novagen
pSCRhaB2	Rhamnose-inducible expression vector, Tp^R	45
pTrc99A	Isopropyl 1-thio-β-D-galactopyranoside-inducible expression vector, Amp^R	GE Healthcare
pCH7590	pET21::*cdiA-CT* (*G123*)-*cdiI$_{II}^{1026b}$*, Amp^R	16
pCH7770	pET21::*cdiA-CT*-*cdiI^{E479}*, Amp^R	16
pCH8479	pET21::*cdiA-CT* (*G123/D214A*)-*cdiI$_{II}^{1026b}$*, Amp^R	16
pCH7913	pET21::*cdiI^{E479}*, Amp^R	16
pCH8288	pET21::*cdiA-CT* (*D285A*)-*cdiI^{E479}*, Amp^R	16
pCH8427	pET21::*cdiA-CT* (*G157/D285A*)-*cdiI^{E479}*, Amp^R	16
pPJ100	pET28::*his$_6$*-*cdiA-CT* (*G157/D243A/D285A*)^{E479}, Amp^R	This study
pCH10115	pET21::*his$_6$*-*cdiA-CT* (*G123/D214A*)^{1026b}, Amp^R	This study
pCH11617	pET21::*cdiA-CT* (*D229A*)-*cdiI^{E479}*, Amp^R	This study
pCH11618	pET21::*cdiA-CT* (*H275A*)-*cdiI^{E479}*, Amp^R	This study
pCH11619	pET21::*cdiA-CT* (*D243A*)-*cdiI^{E479}*, Amp^R	This study
pCH11620	pET21::*cdiA-CT* (*E204A*)-*cdiI^{E479}*, Amp^R	This study
pCH11648	pSCRhaB::*cdiA-CT* (*D229A*)^{E479}, Tp^R	This study
pCH11649	pSCRhaB::*cdiA-CT* (*H275A*)^{E479}, Tp^R	This study
pCH11650	pSCRhaB::*cdiA-CT* (*D243A*)^{E479}, Tp^R	This study
pCH11651	pSCRhaB::*cdiA-CT* (*E204A*)^{E479}, Tp^R	This study
pCH11669	pSCRhaB::*cdiA-CT^{E479}*, Tp^R	This study

[a] The abbreviations used are as follows: Amp^R, ampicillin-resistant; Kan^R, kanamycin-resistant; Rif^R, rifampicin-resistant; Tp^R, trimethoprim-resistant.

studies reported here represent the first steps toward a detailed understanding of tRNA-binding specificity. Docking of tRNA onto the CdiA-CT^{1026b} domain provides a reasonable model for toxin binding to the aminoacyl-acceptor stem. The interaction between CdiA-CT^{E479} and substrate appears to be more complicated, and it is unclear why CdiA-CT^{E479}/tRNA complexes oligomerize in solution. It should be noted that CdiA-CT^{E479} in the absence of tRNA also forms a tetramer (data not shown). Although the models are still vague, it is tempting to speculate that the additional helix α2a within CdiA-CT^{E479} contributes to T-loop binding specificity. Helix α2a forms a ridge along the lower edge of the putative tRNA-binding surface. Residues Phe-260 and Phe-261, which form a prominent hydrophobic patch adjacent to the nuclease-active site, may participate in substrate binding by stacking onto nucleobases. An elucidation of specific contacts must await high resolution structural studies of toxin/substrate complexes. Given that inactive versions of each nuclease domain bind to tRNA with high affinity, it should be possible to generate specific nucleoprotein complexes for high resolution crystallography.

We have now reported crystal structures for four different CDI toxin classes. As described above, three of these toxins are nucleases of the PD(D/E)*X*K superfamily. The other toxin, CdiA-CT^{ECL} from *Enterobacter cloacae* ATCC 13047, is an Ntox21 family member and adopts a fold common to barnase, endonuclease poly(U)-specific, colicin E5/D, and RelE (BECR) toxins (14, 26). Sequence analyses by Aravind and co-workers (14, 15) indicate that CDI systems encode several other toxin families with distinct protein folds and activities. However, most CdiA-CT sequences do not have Pfam designations nor predictions for their biochemical activities (3). Given that the CdiA-CT^{E479}, CdiA-CT^{1026b}, and CdiA-CT^{YPIII} toxins were not identified as PD(D/E)*X*K nucleases by prior computational surveys, it remains possible that other uncharacterized CDI toxins also belong to the superfamily. Because of extreme sequence variability and catalytic residue migration, PD(D/E)*X*K enzymes are notoriously difficult to identify through computational approaches (23, 25, 38). This problem is compounded by insertions and circular permutations of the core structure (23). Aravind and co-workers (14) recently predicted five new restriction endonuclease-like domains (Tox-REase-2, -3, -5, -7, and -9) that are associated with prokaryotic competition systems. Only the Tox-REase-7 family (Pfam PF15649) is found in CdiA effectors, and these CDI toxins appear to be limited to *Pseudomonas* and *Acinetobacter* species. These systems are under considerable positive selection to diversify, presumably due to the competitive advantage obtained with novel toxins. Similar pressures are postulated to drive the impressive diversity of restriction endonucleases, which is the result of the complex interplay between bacteria and their phages (44). Thus, it is not surprising that the versatile PD(D/E)*X*K core structure has been adopted by CDI and other prokaryotic competition systems.

Experimental Procedures

Plasmid Constructions—Plasmids used in this study are listed in Table 4. Constructs for the overproduction of CdiA-CT/CdiI^{1026b}-His$_6$ (pCH7590), CdiA-CT(D285A)/CdiI^{E479}-His$_6$ (pCH8288), and wild-type CdiA-CT/CdiI^{E479}-His$_6$ (pCH7770) complexes have been described previously (16). Active-site mutations were made in the CdiA-CT^{E479} nuclease domain using mega-primer PCR. Plasmid pCH7770 was amplified with primer E479-cdiI-Spe-rev (5′-TTT ACT AGT ATT CCC CGA AAC TCC GAG CC) in conjunction with mutagenic forward primers: E479-E204A-for (5′-AAA TTT AGA CCA GGT GCA GCC GGA GCA GCG GC), E479-D229A-for (5′-GGC TCC TCG GTT GCC TTT GTA TTC AGC TCC), E479-D243A-for (5′-AAC GGT AAG ACC GTG GCT TTT ATG CTT ACG CC), and E479-H275A-for (5′-GAA CAC TCT TTC GGA TGC

TGC GGC TGC TGC GG). The resulting products were used as mega-primers in subsequent reactions with forward primer E479-Nco-for (5′-CGG CCA TGG CAT CGA ACG TCG AGC TTT AC). The final products were digested with NcoI and SpeI and then ligated to plasmid pET21 to generate mutant CdiA-CT/CdiI^{E479}-His$_6$ expression constructs. These plasmids were used as templates to amplify *cdiA-CT*^{E479} coding sequences with primers E479-Nco-for and E479-CT-Xho-rev (5′-GCC ACT CGA GCC TTA CTT GAT CAG AAT AAT C). The products were digested with NcoI and XhoI and then ligated to plasmid pSCRhaB2 (45) to generate L-rhamnose-inducible expression constructs to monitor growth inhibition activities. Plasmid pCH8479 was amplified with oligonucleotides 1026b-Spe-for (5′-ATA ACT AGT GCA TCG AAC GTC GAG C) and 1026b-CT-Xho-rev (5′-AAT CTC GAG TTA ATT CCC CTT TGG), and the resulting fragment was ligated into plasmid pSH21 to generate a construct that overproduces inactive His$_6$-CdiA-CT(D214A)^{1026b}. The *cdiA-CT*(*D285A*)^{E479} coding sequence was amplified from pCH8427 with primers E479-CT-NdeI-H6-for (5′-GAT CAT ATG ATG GGG GCA AGC TCA GGT AGT AAT ATC) and E479-CT-EcoRI-rev (5′-GAT GAA TTC TCA CTT GAT CAG AAT AAT CTT CGC CTG CAG TTT). The product was digested with NdeI/EcoRI and ligated to pET28b. The D243A mutation was introduced via site-directed mutagenesis using primers E479-CT-D243A-for (5′-CGG TAA GAC CGT GGC GTT TAT GCT TAC GCC-3′) and E479-CT-D243A-rev (5′-GGC GTA AGC ATA AAC GCC ACG GTC TTA CCG-3′) to produce an expression construct that overproduces His$_6$-CdiA-CT^{E479} carrying the D243A and D285A mutations.

Protein Overexpression and Purification—CdiA-CT^{E479} (from residue Gly-157, numbered from Glu-1 of the ELYN motif) was co-expressed with CdiI^{E479}-His$_6$ and overproduced in *E. coli* BL21 (DE3) cells grown aerobically at 37 °C in LB medium supplemented with 50 μg/ml ampicillin. Protein expression was induced by addition of isopropyl β-D-thiogalactoside to 1 mM final concentration once the culture reached an absorbance at 600 nm (A_{600}) of ~0.8. Induced cells were incubated for 4 h and then harvested by centrifugation at 5,100 × *g* for 20 min. The cell pellet was resuspended in 20 mM sodium phosphate (pH 7.0), 200 mM NaCl supplemented with 10 mg/ml lysozyme, and 1 mM phenylmethylsulfonyl fluoride (PMSF), and the cells were broken by sonication. The lysate was clarified by centrifugation at 14,000 × *g* for 30 min, and the soluble fraction passed through a 0.22-μm filter before loading onto a Ni^{2+}-charged Hi-trap column (GE Healthcare). The column was washed with 20 mM sodium phosphate (pH 7.0), 200 mM NaCl, 15 mM imidazole, and the CdiA-CT/CdiI^{E479}-His$_6$ complex eluted with a linear gradient of 15–250 mM imidazole. The purified complex was concentrated with a 10-kDa centrifugal concentrator and then run on a Superdex 200 size-exclusion column equilibrated in 50 mM Tris-HCl (pH 7.4), 150 mM NaCl. SeMet-labeled proteins were overproduced in *E. coli* BL21 (DE3) cells grown in M9 minimal medium supplemented with L-leucine, L-isoleucine, and L-valine at 50 mg/liter; L-phenylalanine, L-lysine, and L-threonine at 100 mg/liter; and SeMet at 75 mg/liter as described (46). The SeMet-labeled CdiA-CT/CdiI^{E479}-His$_6$ complex was purified as described above.

Crystallization and Structure Determination—CdiA-CT/CdiI^{E479} was crystallized by hanging drop-vapor diffusion against a 1-ml reservoir of crystallization buffer (0.1 M HEPES (pH 7.0), 20 mM $MgCl_2$, 30% (w/v) polyacrylic acid). Polyacrylic acid (Sigma) with average molecular mass of 5,100 Da was prepared as a 50% (w/v) solution, filtered, and used to facilitate crystallization. Hanging drops were prepared from a 1:1 (v/v) mixture of protein solution (20 mg/ml) and crystallization buffer supplemented with 20 μg/ml chymotrypsin. Crystals were soaked in cryo-protectant solution containing 1:1 mixture of 40% (v/v) glycerol and crystallization buffer and then collected by flash freezing. A native dataset was acquired at 70 K at 0.97591 Å on beamline 7-1 at Stanford Synchrotron Radiation Lightsource. Data were processed using HKL2000 (47), resulting in a 99.24% complete dataset to 2.0 Å resolution. The CdiA-CT/CdiI^{E479} complex crystallized in space group $P22_12_1$ with two complexes per asymmetric unit and unit cell dimensions of 54.5 × 73.3 × 110.0 Å. Diffraction data were initially indexed and scaled to $P222_1$; however, the best solution obtained by molecular replacement using Phaser in the PHENIX suite was $P22_12_1$. The SeMet-labeled complex was crystallized using 0.1 M MES (pH 6.5), 0.01 M $ZnCl_2$, 15% (w/v) PEG-6000 as the buffer. SeMet-labeled CdiA-CT/CdiI^{E479} crystallized in space group I4 with three complexes per asymmetric unit and unit cell dimensions of 117.2 × 117.2 × 111.6 Å. A SAD was collected at 70 K at 0.97591 Å on beamline 7-1 at Stanford Synchrotron Radiation Lightsource. Data were processed using HKL2000, yielding a 99.9% complete dataset to 3.3 Å resolution. We used Autosol in the PHENIX suite (48) to detect 18 selenium atoms with a figure of merit of 0.408 and overall score of 36.2 ± 14.2. Autosol also built a partial model consisting of 416 residues with an R_{work}/R_{free} (%) of 38.4/44.9. This model showed little secondary structure except for α1 of CdiA-CT^{E479} and α2′ and α3′ of CdiI^{E479}. Molecular replacement was carried out with Phaser in the PHENIX suite using the partial model together with higher resolution data from native crystals. The Phaser-generated model was then subjected to Autobuild and phenix.refine (48). The final model includes residues Arg-201–Lys-316 of CdiA-CT^{E479} and residues Ala-2–Gly-105 of CdiI^{E479} with a final R_{work}/R_{free} (%) 19.3/23.7. The Ramachandran plot shows 98.8% in the favorable allowed regions and the other 1.2% in the allowed regions. Data collection and refinement statistics are presented in Table 1. Intermolecular hydrogen bonds and salt bridges were determined using PDBePISA (49).

Toxin Immunity Protein Binding Kinetics—The apparent equilibrium dissociation constant for the CdiA-CT/CdiI^{E479} complex was determined by biolayer interferometry using a BLitz instrument (ForteBio) (50). CdiA-CT^{E479} was separated from CdiI^{E479}-His$_6$ by Ni^{2+}-affinity chromatography under denaturing conditions. The isolated toxin was refolded by dialysis and run on a Superdex S200 size-exclusion column. CdiI^{E479}-His$_6$ was purified by Ni^{2+}-affinity chromatography as described previously (16). CdiI^{E479}-His$_6$ was loaded onto a Ni^{2+}-NTA-coated biosensor in 50 mM Tris-HCl (pH 7.4), 150 mM NaCl at 25 °C. Sensor-bound immunity protein was then incubated with

TABLE 5
Data collection and scattering-derived parameters for tRNA·CdiA-CT complexes

Data collection parameters	tRNA/CdiA-CT^{1026b}	tRNA/CdiA-CT^{E479}
Beam line	ALS 12.3.1	ALS 12.3.1
Wavelength (Å)	1.0	1.0
q range (Å^{-1})	0.012–0.324	0.012–0.324
Exposure time (seconds)	0.5, 1, 2, 4	0.5, 1, 2, 4
Concentration range (mg ml^{-1})	0.5–5	2–10
Temperature (K)	283	283
Structural parameters[a]		
$I(0)$ (cm^{-1}) (from $P(r)$)	248.1 ± 13.2	595.9 ± 13.4
R_g (Å) (from $P(r)$)	27.3 ± 1.3	46.9 ± 3.4
$I(0)$ (cm^{-1}) (from Guinier)	246.8 ± 14.9	590.6 ± 20.8
R_g (Å) (from Guinier)	27.1 ± 1.7	46.1 ± 4.0
D_{max} (Å)[b]	91	190
Porod volume estimate (Å^3)	43,041 ± 2,353	256,350 ± 2,517
Dry volume calculated from Crysol[14] (Å^3)[c]	45,510	43,112 (176,000)[d]
Molecular mass determination[a]		
Molecular mass (from Primus) (Da)	41,539 ± 1,675	16,5473 ± 6,083
Calculated monomeric mass from sequence (Da)[c]	43,215	41,827 (167,308)

[a] Data are reported for 5 mg ml^{-1} measurements.
[b] D_{max} is a model parameter in the $P(r)$ calculation.
[c] Values for tetramer are shown in parentheses.
[d] The estimated volume of the tRNA·CdiA-CT^{E479} complex is greater than the calculated volume from sequence due to the void volume assumed by the tetramer.

1.5–5 μM CdiA-CT^{E479} toxin for 180 s. The sensor was then washed with buffer, and toxin dissociation was monitored over 180 s. Curve fitting was run following reference subtraction using the BLitz Pro Software to calculate dissociation constants. Local fit analyses were performed for individual association-dissociation curves, followed by averaging to obtain the final apparent K_d value and standard deviation.

Growth Inhibition Assays—*E. coli* X90 cells harboring rhamnose-inducible CdiA-CT^{E479} expression plasmids (Table 4) were grown to mid-log phase in LB media supplemented with 100 μg/ml trimethoprim. Cells were then diluted to $A_{600} = 0.05$ in fresh LB media supplemented with 100 μg/ml trimethoprim and either 0.4% D-glucose to repress or 0.4% L-rhamnose to induce CdiA-CT^{E479} expression. Cultures were incubated with shaking at 37 °C, and cell growth was monitored by measuring the A_{600} every 30 min.

In Vitro tRNase Assays—Purified CdiA-CT/CdiI^{E479}-His$_6$ complexes were denatured in binding buffer supplemented with 6 M guanidine-HCl and CdiA-CT^{E479} isolated from the void volume during Ni^{2+}-affinity chromatography (1). Toxins were refolded by dialysis against binding buffer, and all purified proteins were quantified by absorbance at 280 nm. Total RNA was isolated from *E. coli* X90 cells as described (51) and used as a substrate for *in vitro* nuclease assays. *E. coli* RNA (5 μg) was incubated with CdiA-CT^{E479} variants (5 μM) in reaction buffer (20 mM Tris-HCl (pH 7.5), 100 mM NaCl, 10 mM $MgCl_2$, 0.2 mg/ml BSA) for 1 h at 37 °C. Where indicated, CdiI^{E479} was included at 17.5 μM final concentration. tRNA^{Asp} and tRNA^{Gln} substrates were generated by *in vitro* transcription using RNA polymerase from bacteriophage T7 RNA. The tRNA^{Asp} template was prepared with oligonucleotides 5′-tRNA-Asp (5′-AAT TCC TGC AGT AAT ACG ACT CAC TAT AGG AGC GGT AGT TCA GTC GGT TAG AAT ACC TG) and 3′-tRNA-Asp (5′-TGG CGG AAC GGA CGG GAC TCG AAC CCG CGA CCC CCT GCG TGA CAG GCA GGT ATT CTA AC), and the tRNA^{Gln} template with oligonucleotides 5′-tRNA-Gln (5′-AAT TCC TGC AGT AAT ACG ACT CAC TAT AGG GGG TAT AGG GGG TAT CGC CAA GCG GTA AGG CAC CGG) and 3′-tRNA-Gln (5′-TGG CTG GGG TAC GAG GAT TCG AAC CTC GGA ATG CCG GAA TCA GAA TCC GGT GCC TT). Annealed oligonucleotides were end-filled with Klenow fragment of DNA polymerase I. Templates were incubated with T7 RNA polymerase, 2 mM NTP, 10 mM dithiothreitol, and 10 mM $MgCl_2$ for 3 h at 37 °C. Template DNA was removed with RNase-free DNase I, and the transcripts purified with the Direct-zol RNA MiniPrep kit (Genesee Scientific). Nuclease reactions were analyzed by denaturing electrophoresis on 50% urea, 6% polyacrylamide gels in 1× Tris borate-EDTA (TBE) buffer. Gels were stained with ethidium bromide or transferred to nylon membrane for Northern blot hybridization with 5′-radiolabeled oligonucleotide glyV probe (5′-CTT GGC AAG GTC GTG CT) as described (16, 51).

Molecular Docking—Hex 8.0 (52–54) was used to dock CdiA-CT nuclease domains onto tRNA to generate models of enzyme/substrate complexes. CdiA-CT^{1026b} and CdiA-CT^{E479} nuclease domains were docked onto the structure of *E. coli* tRNA^{Cys} (PDB code 1B23) (55). The active site of each nuclease was positioned adjacent to the known scissile bond and the origin set to sample multiple orientations in search of the low energy interactions. Positive control docking simulations were performed using cognate and non-cognate toxin/immunity proteins pairs from *B. pseudomallei* E479 and 1026b. As a negative control, CdiI^{E479} and CysK from *Salmonella typhimurium* LT2 (PDB code 1OAS (56)) were docked onto one another.

SAXS—Inactive CdiA-CT(D243A/D285A)^{E479} and CdiA-CT(D214A)^{1026b} (17) toxins carrying N-terminal His$_6$ epitope tags were purified by Ni^{2+}-affinity chromatography under non-denaturing conditions. Under these conditions, endogenous tRNA co-purifies with the inactive nuclease domains. Toxin/tRNA complexes were exchanged into 20 mM sodium phosphate (pH 7.4), 150 mM NaCl using a Superdex S200 size-exclusion column and diluted to several concentrations ranging from 0.5 to 5 mg/ml for SAXS analysis. SAXS data were collected on SIBYLS beamline 12.3.1 at the Advanced Light Source using a Pilatus3 2 M detector with exposure times of 0.5, 1, 2, and 4 s. Buffer subtracted data were analyzed using PRIMUS (31), following modification with GNOM (57); $P(r)$ output files with

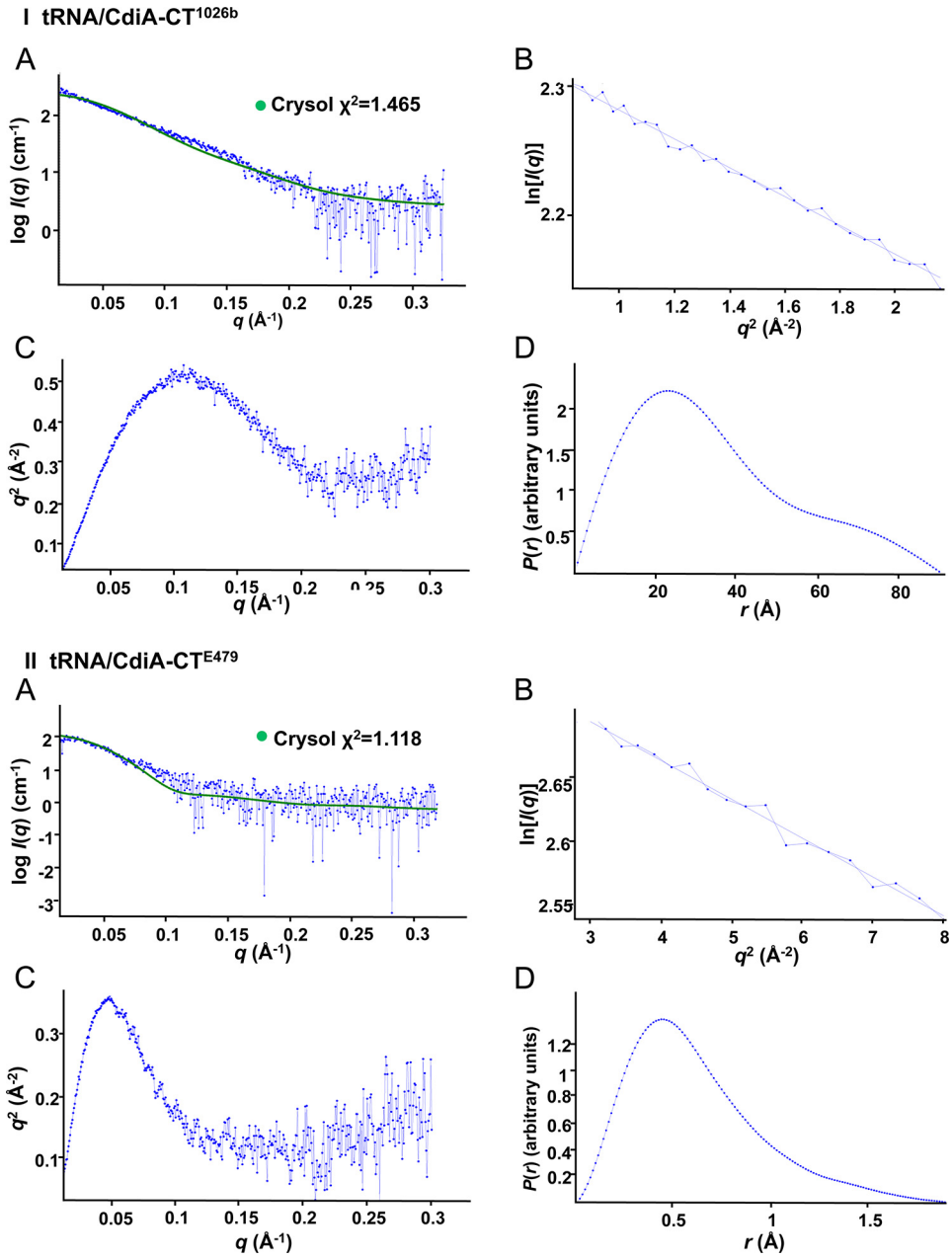

FIGURE 9. **SAXS analyses of tRNA/CdiA-CT complexes.** Plots for tRNA/CdiA-CT^{1026b} (*I*) and tRNA/CdiA-CT^{E479} (*II*) SAXS data. *A*, log *I*(*q*) *versus q* plot with experimental SAXS profile shown in *blue* and the corresponding structural model fitted data via Crysol (41) shown in *green*. *B*, Guinier plots. *C*, Kratky plots. *D*, *P*(*r*) plots.

d^{max} of 91 and 190 for tRNA/CdiA-CT^{1026b} and tRNA/CdiA-CT^{E479} complexes (respectively) were used to generate electron density envelopes via GASBOR (58). Density envelopes (12 per tRNA/toxin complex) were averaged using DAMAVER (31), and docking solutions were fitted into the final envelopes using Chimera (32) and Crysol (59). SAXS parameters and statistics are provided in Table 5 according to (60). Crysol outputs, together with Guinier, Kratky and *P(r)* plots, are presented in Fig. 9.

Author Contributions—P. M. J., G. C. G., F. G.-S., T. W., L.-W. H., C. S. H., and C.W.G. conceived and designed experiments and analyzed data; P. M. J., G. C. G., F. G.-S., T. W., and L.-W. H. performed the experiments; P. M. J., G. C. G., F. G.-S., T. W., L.-W. H., C. S. H., and C. W. G. wrote the paper.

Acknowledgments—We thank the Stanford Synchrotron Radiation Lightsource for their invaluable help in data collection. We thank the beam line staff members at the beam lines 12.3.1 (BL12.3.1) at the Advanced Light Source for their help in SAXS data collection. The Advanced Light Source is operated by Lawrence Berkeley National Laboratory on behalf of the Department of Energy, Office of Basic Energy Sciences, through the Integrated Diffraction Analysis Technologies program, supported by Department of Energy, Office of Biological and Environmental Research.

References

1. Aoki, S. K., Diner, E. J., de Roodenbeke, C. T., Burgess, B. R., Poole, S. J., Braaten, B. A., Jones, A. M., Webb, J. S., Hayes, C. S., Cotter, P. A., and Low,

D. A. (2010) A widespread family of polymorphic contact-dependent toxin delivery systems in bacteria. *Nature* **468,** 439–442
2. Ruhe, Z. C., Low, D. A., and Hayes, C. S. (2013) Bacterial contact-dependent growth inhibition. *Trends Microbiol.* **21,** 230–237
3. Willett, J. L., Ruhe, Z. C., Goulding, C. W., Low, D. A., and Hayes, C. S. (2015) Contact-dependent growth inhibition (CDI) and CdiB/CdiA two-partner secretion proteins. *J. Mol. Biol.* **427,** 3754–3765
4. Makhov, A. M., Hannah, J. H., Brennan, M. J., Trus, B. L., Kocsis, E., Conway, J. F., Wingfield, P. T., Simon, M. N., and Steven, A. C. (1994) Filamentous hemagglutinin of *Bordetella pertussis.* A bacterial adhesin formed as a 50-nm monomeric rigid rod based on a 19-residue repeat motif rich in β strands and turns. *J. Mol. Biol.* **241,** 110–124
5. Kajava, A. V., Cheng, N., Cleaver, R., Kessel, M., Simon, M. N., Willery, E., Jacob-Dubuisson, F., Locht, C., and Steven, A. C. (2001) β-Helix model for the filamentous haemagglutinin adhesin of *Bordetella pertussis* and related bacterial secretory proteins. *Mol. Microbiol.* **42,** 279–292
6. Aoki, S. K., Malinverni, J. C., Jacoby, K., Thomas, B., Pamma, R., Trinh, B. N., Remers, S., Webb, J., Braaten, B. A., Silhavy, T. J., and Low, D. A. (2008) Contact-dependent growth inhibition requires the essential outer membrane protein BamA (YaeT) as the receptor and the inner membrane transport protein AcrB. *Mol. Microbiol.* **70,** 323–340
7. Ruhe, Z. C., Townsley, L., Wallace, A. B., King, A., Van der Woude, M. W., Low, D. A., Yildiz, F. H., and Hayes, C. S. (2015) CdiA promotes receptor-independent intercellular adhesion. *Mol. Microbiol.* **98,** 175–192
8. Ruhe, Z. C., Wallace, A. B., Low, D. A., and Hayes, C. S. (2013) Receptor polymorphism restricts contact-dependent growth inhibition to members of the same species. *mBio* **4,** e00480–e00413
9. Aoki, S. K., Pamma, R., Hernday, A. D., Bickham, J. E., Braaten, B. A., and Low, D. A. (2005) Contact-dependent inhibition of growth in *Escherichia coli. Science* **309,** 1245–1248
10. Aoki, S. K., Poole, S. J., Hayes, C. S., and Low, D. A. (2011) Toxin on a stick: modular CDI toxin delivery systems play roles in bacterial competition. *Virulence* **2,** 356–359
11. Hayes, C. S., Aoki, S. K., and Low, D. A. (2010) Bacterial contact-dependent delivery systems. *Annu. Rev. Genet.* **44,** 71–90
12. Poole, S. J., Diner, E. J., Aoki, S. K., Braaten, B. A., t'Kint de Roodenbeke, C., Low, D. A., and Hayes, C. S. (2011) Identification of functional toxin/immunity genes linked to contact-dependent growth inhibition (CDI) and rearrangement hotspot (Rhs) systems. *PLoS Genet.* **7,** e1002217
13. Webb, J. S., Nikolakakis, K. C., Willett, J. L., Aoki, S. K., Hayes, C. S., and Low, D. A. (2013) Delivery of CdiA nuclease toxins into target cells during contact-dependent growth inhibition. *PLoS ONE* **8,** e57609
14. Zhang, D., de Souza, R. F., Anantharaman, V., Iyer, L. M., and Aravind, L. (2012) Polymorphic toxin systems: comprehensive characterization of trafficking modes, processing, mechanisms of action, immunity and ecology using comparative genomics. *Biol. Direct.* **7,** 18
15. Zhang, D., Iyer, L. M., and Aravind, L. (2011) A novel immunity system for bacterial nucleic acid degrading toxins and its recruitment in various eukaryotic and DNA viral systems. *Nucleic Acids Res.* **39,** 4532–4552
16. Nikolakakis, K., Amber, S., Wilbur, J. S., Diner, E. J., Aoki, S. K., Poole, S. J., Tuanyok, A., Keim, P. S., Peacock, S., Hayes, C. S., and Low, D. A. (2012) The toxin/immunity network of *Burkholderia pseudomallei* contact-dependent growth inhibition (CDI) systems. *Mol. Microbiol.* **84,** 516–529
17. Morse, R. P., Nikolakakis, K. C., Willett, J. L., Gerrick, E., Low, D. A., Hayes, C. S., and Goulding, C. W. (2012) Structural basis of toxicity and immunity in contact-dependent growth inhibition (CDI) systems. *Proc. Natl. Acad. Sci. U.S.A.* **109,** 21480–21485
18. Lazar Adler, N. R., Govan, B., Cullinane, M., Harper, M., Adler, B., and Boyce, J. D. (2009) The molecular and cellular basis of pathogenesis in melioidosis: how does *Burkholderia pseudomallei* cause disease? *FEMS Microbiol. Rev.* **33,** 1079–1099
19. Limmathurotsakul, D., and Peacock, S. J. (2011) Melioidosis: a clinical overview. *Br. Med. Bull.* **99,** 125–139
20. Chantratita, N., Wuthiekanun, V., Limmathurotsakul, D., Vesaratchavest, M., Thanwisai, A., Amornchai, P., Tumapa, S., Feil, E. J., Day, N. P., and Peacock, S. J. (2008) Genetic diversity and microevolution of *Burkholderia pseudomallei* in the environment. *PLoS Negl. Trop. Dis.* **2,** e182
21. Ngamdee, W., Tandhavanant, S., Wikraiphat, C., Reamtong, O., Wuthiekanun, V., Salje, J., Low, D. A., Peacock, S. J., and Chantratita, N. (2015) Competition between *Burkholderia pseudomallei* and *B. thailandensis. BMC Microbiol.* **15,** 56
22. Ogawa, T., Tomita, K., Ueda, T., Watanabe, K., Uozumi, T., and Masaki, H. (1999) A cytotoxic ribonuclease targeting specific transfer RNA anticodons. *Science* **283,** 2097–2100
23. Steczkiewicz, K., Muszewska, A., Knizewski, L., Rychlewski, L., and Ginalski, K. (2012) Sequence, structure and functional diversity of PD(D/E)XK phosphodiesterase superfamily. *Nucleic Acids Res.* **40,** 7016–7045
24. Holm, L., and Rosenström, P. (2010) Dali server: conservation mapping in 3D. *Nucleic Acids Res.* **38,** W545–W549
25. Kosinski, J., Feder, M., and Bujnicki, J. M. (2005) The PD(D/E)XK superfamily revisited: identification of new members among proteins involved in DNA metabolism and functional predictions for domains of (hitherto) unknown function. *BMC Bioinformatics* **6,** 172
26. Beck, C. M., Morse, R. P., Cunningham, D. A., Iniguez, A., Low, D. A., Goulding, C. W., and Hayes, C. S. (2014) CdiA from *Enterobacter cloacae* delivers a toxic ribosomal RNase into target bacteria. *Structure* **22,** 707–718
27. Morse, R. P., Willett, J. L., Johnson, P. M., Zheng, J., Credali, A., Iniguez, A., Nowick, J. S., Hayes, C. S., and Goulding, C. W. (2015) Diversification of β-augmentation interactions between CDI toxin/immunity proteins. *J. Mol. Biol.* **427,** 3766–3784
28. Willett, J. L., Gucinski, G. C., Fatherree, J. P., Low, D. A., and Hayes, C. S. (2015) Contact-dependent growth inhibition toxins exploit multiple independent cell-entry pathways. *Proc. Natl. Acad. Sci. U.S.A.* **112,** 11341–11346
29. Yang, X., Tan, S. H., Teh, Y. J., and Yuan, Y. A. (2011) Structural implications into dsRNA binding and RNA silencing suppression by NS3 protein of Rice Hoja Blanca Tenuivirus. *RNA* **17,** 903–911
30. Hemmes, H., Lakatos, L., Goldbach, R., Burgyán, J., and Prins, M. (2007) The NS3 protein of Rice hoja blanca tenuivirus suppresses RNA silencing in plant and insect hosts by efficiently binding both siRNAs and miRNAs. *RNA* **13,** 1079–1089
31. Konarev, P. V., Volkov, V. V., Sokolova, A. V., Koch, M. H., and Svergun, D. I. (2003) PRIMUS: a Windows PC-based system for small-angle scattering data analysis. *J. Appl. Crystallogr.* **36,** 1277–1282
32. Pettersen, E. F., Goddard, T. D., Huang, C. C., Couch, G. S., Greenblatt, D. M., Meng, E. C., and Ferrin, T. E. (2004) UCSF Chimera–a visualization system for exploratory research and analysis. *J. Comput. Chem.* **25,** 1605–1612
33. Kozin, M. B., and Svergun, D. I. (2001) Automated matching of high- and low-resolution structural models. *J. Appl. Cryst.* **34,** 33–41
34. Nooren, I. M., and Thornton, J. M. (2003) Structural characterisation and functional significance of transient protein-protein interactions. *J. Mol. Biol.* **325,** 991–1018
35. Moras, D., Comarmond, M. B., Fischer, J., Weiss, R., Thierry, J. C., Ebel, J. P., and Giegé, R. (1980) Crystal structure of yeast tRNAAsp. *Nature* **288,** 669–674
36. Pingoud, A., and Jeltsch, A. (2001) Structure and function of type II restriction endonucleases. *Nucleic Acids Res.* **29,** 3705–3727
37. Knizewski, L., Kinch, L. N., Grishin, N. V., Rychlewski, L., and Ginalski, K. (2007) Realm of PD(D/E)XK nuclease superfamily revisited: detection of novel families with modified transitive meta profile searches. *BMC Struct. Biol.* **7,** 40
38. Gupta, R., Capalash, N., and Sharma, P. (2012) Restriction endonucleases: natural and directed evolution. *Appl. Microbiol. Biotechnol.* **94,** 583–599
39. Kachalova, G. S., Rogulin, E. A., Yunusova, A. K., Artyukh, R. I., Perevyazova, T. A., Matvienko, N. I., Zheleznaya, L. A., and Bartunik, H. D. (2008) Structural analysis of the heterodimeric type IIS restriction endonuclease R. BspD6I acting as a complex between a monomeric site-specific nickase and a catalytic subunit. *J. Mol. Biol.* **384,** 489–502
40. Hashimoto, H., Shimizu, T., Imasaki, T., Kato, M., Shichijo, N., Kita, K., and Sato, M. (2005) Crystal structures of type II restriction endonuclease EcoO109I and its complex with cognate DNA. *J. Biol. Chem.* **280,** 5605–5610
41. Feder, M., and Bujnicki, J. M. (2005) Identification of a new family of

putative PD(D/E)XK nucleases with unusual phylogenomic distribution and a new type of the active site. *BMC Genomics* **6,** 21
42. Bujnicki, J. M., and Rychlewski, L. (2001) Unusual evolutionary history of the tRNA splicing endonuclease EndA: relationship to the LAGLIDADG and PD(D/E)XK deoxyribonucleases. *Protein Sci.* **10,** 656–660
43. Jiao, X., Xiang, S., Oh, C., Martin, C. E., Tong, L., and Kiledjian, M. (2010) Identification of a quality-control mechanism for mRNA 5′-end capping. *Nature* **467,** 608–611
44. Stern, A., and Sorek, R. (2011) The phage-host arms race: shaping the evolution of microbes. *BioEssays* **33,** 43–51
45. Cardona, S. T., and Valvano, M. A. (2005) An expression vector containing a rhamnose-inducible promoter provides tightly regulated gene expression in *Burkholderia cenocepacia*. *Plasmid* **54,** 219–228
46. Van Duyne, G. D., Standaert, R. F., Karplus, P. A., Schreiber, S. L., and Clardy, J. (1993) Atomic structures of the human immunophilin FKBP-12 complexes with FK506 and rapamycin. *J. Mol. Biol.* **229,** 105–124
47. Otwinowski, Z., and Minor, W. (1997) Processing of x-ray diffraction data collected in oscillation mode. *Methods Enzymol.* **276,** 307–326
48. Terwilliger, T. C., Adams, P. D., Read, R. J., McCoy, A. J., Moriarty, N. W., Grosse-Kunstleve, R. W., Afonine, P. V., Zwart, P. H., and Hung, L. W. (2009) Decision-making in structure solution using Bayesian estimates of map quality: the PHENIX AutoSol wizard. *Acta Crystallogr. D Biol. Crystallogr.* **65,** 582–601
49. Krissinel, E., and Henrick, K. (2007) Inference of macromolecular assemblies from crystalline state. *J. Mol. Biol.* **372,** 774–797
50. Concepcion, J., Witte, K., Wartchow, C., Choo, S., Yao, D., Persson, H., Wei, J., Li, P., Heidecker, B., Ma, W., Varma, R., Zhao, L. S., Perillat, D., Carricato, G., Recknor, M., *et al.* (2009) Label-free detection of biomolecular interactions using BioLayer interferometry for kinetic characterization. *Comb. Chem. High Throughput Screen.* **12,** 791–800
51. Garza-Sánchez, F., Janssen, B. D., and Hayes, C. S. (2006) Prolyl-tRNA(Pro) in the A-site of SecM-arrested ribosomes inhibits the recruitment of transfer-messenger RNA. *J. Biol. Chem.* **281,** 34258–34268
52. Ritchie, D. W. (2003) Evaluation of protein docking predictions using Hex 3.1 in CAPRI rounds 1 and 2. *Proteins* **52,** 98–106
53. Ritchie, D. W., and Kemp, G. J. (2000) Protein docking using spherical polar Fourier correlations. *Proteins* **39,** 178–194
54. Ritchie, D. W., and Venkatraman, V. (2010) Ultra-fast FFT protein docking on graphics processors. *Bioinformatics* **26,** 2398–2405
55. Nissen, P., Thirup, S., Kjeldgaard, M., and Nyborg, J. (1999) The crystal structure of Cys-tRNACys-EF-Tu-GDPNP reveals general and specific features in the ternary complex and in tRNA. *Structure* **7,** 143–156
56. Burkhard, P., Rao, G. S., Hohenester, E., Schnackerz, K. D., Cook, P. F., and Jansonius, J. N. (1998) Three-dimensional structure of *O*-acetylserine sulfhydrylase from *Salmonella typhimurium*. *J. Mol. Biol.* **283,** 121–133
57. Svergun, D. I. (1992) Determination of the regularization parameter in indirect-transform methods using perceptual criteria. *J. Appl. Crystallogr.* **25,** 495–503
58. Svergun, D. I., Petoukhov, M. V., and Koch, M. H. (2001) Determination of domain structure of proteins from x-ray solution scattering. *Biophys. J.* **80,** 2946–2953
59. Stovgaard, K., Andreetta, C., Ferkinghoff-Borg, J., and Hamelryck, T. (2010) Calculation of accurate small angle x-ray scattering curves from coarse-grained protein models. *BMC Bioinformatics* **11,** 429
60. Jacques, D. A., Guss, J. M., Svergun, D. I., and Trewhella, J. (2012) Publication guidelines for structural modelling of small-angle scattering data from biomolecules in solution. *Acta Crystallogr. D Biol. Crystallogr.* **68,** 620–626
61. Beckwith, J. R., and Signer, E. R. (1966) Transposition of the *lac* region of *Escherichia coli*. I. Inversion of the *lac* operon and transduction of *lac* by phi80. *J. Mol. Biol.* **19,** 254–265